International Journal of Heat and Mass Transfer 65 (2013) 203–218

Contents lists available at SciVerse ScienceDirect

International Journal of Heat and Mass Transfer

journal homepage: www.elsevier.com/locate/ijhmt

Criteria for negating the influence of gravity on flow boiling critical heat flux with two-phase inlet conditions

Christopher Konishi [a], Issam Mudawar [a,*], Mohammad M. Hasan [b]

[a] Boiling and Two-Phase Flow Laboratory (BTPFL), School of Mechanical Engineering, Purdue University, 585 Purdue Mall, West Lafayette, IN 47907, USA
[b] NASA Glenn Research Center, 21000 Brookpark Road, Cleveland, OH 44135, USA

ARTICLE INFO

Article history:
Received 9 February 2013
Received in revised form 23 May 2013
Accepted 23 May 2013
Available online 29 June 2013

Keywords:
Flow boiling
Critical heat flux
Flow orientation
Microgravity

ABSTRACT

This study explores the complex flow boiling CHF mechanisms encountered at different orientations relative to Earth's gravity when the fluid is supplied as a two-phase mixture. Using FC-72 as working fluid, different CHF regimes are identified for different orientations, mass velocities and inlet qualities. Low mass velocities are shown to produce the greatest sensitivity to orientation, while high mass velocities greatly reduce this influence, especially for high inlet qualities. It is also shown that the influence of orientation can be negated by simultaneously satisfying three separate criteria: overcoming the influence of gravity perpendicular to the heated wall, overcoming the influence of gravity parallel to the heated wall, and ensuring that the heated wall is sufficiently long to ensure liquid contact. These criteria are combined to determine the minimum mass velocity required to negate gravity effects in both terrestrial and space applications. Exceeding this minimum is of paramount importance to space systems since it enables the implementation of the vast body of published CHF data, correlations and models developed from terrestrial studies for design of thermal management systems for space applications.

1. Introduction

1.1. Transitioning to two-phase thermal management in future space missions

Space systems are increasing in complexity, size and power requirements. A key emphasis of space agencies is to increase the efficiency of power utilization for both space vehicles and future planetary bases by reducing system weight [1,2]. Among the various subsystems comprising any space vehicle or planetary base are several thermal management systems that are crucial to supporting astronaut life and operation of mechanical and electronic hardware. Key among those is the Thermal Control System (TCS), which is responsible for controlling the temperature and humidity of the operating environment. The TCS is responsible for acquiring heat from a number of heat-producing sources, transporting the heat, and rejecting it to deep space by radiation.

While previous space systems, such as NASA's space shuttles, employed a single-phase liquid TCS, weight reduction for future space systems will require transitioning from single-phase liquid to two-phase thermal management [1,2]. The key reason behind this transition is to capitalize on the merits of latent heat of the working fluid rather than sensible heat alone. With this transition, the TCS can take advantage of orders of magnitude enhancement in evaporation and condensation heat transfer coefficients compared to the heat transfer coefficients realized in single-phase liquid systems. For a given total heat load, this transition translates into drastic reductions in weight and volume of the thermal management hardware.

1.2. Gravity effects in boiling systems

Large density difference between liquid and vapor is the primary reason for the strong influence of gravity on two-phase fluid flow and heat transfer. This influence is manifest in the form of a buoyancy force proportional to the product of density difference and gravity. Critical heat flux (CHF) is arguably the most important design parameter for heat-flux-controlled two-phase systems. This explains the great emphasis researchers have placed on measuring, correlating and/or predicting CHF for virtually every two-phase flow configuration, including pool boiling [3,4], channel flow boiling [5–10], jets [11–14], sprays [15–17], and enhanced surfaces [18–20]. The present study concerns CHF in channel flow boiling.

1.3. Influence of orientation on flow boiling CHF

Vertical upflow is a preferred orientation for flow boiling systems because it enables buoyancy to move vapor in the same

* Corresponding author. Tel.: +1 (765) 494 5705; fax: +1 (765) 494 0539.
E-mail address: mudawar@ecn.purdue.edu (I. Mudawar).
URL: https://engineering.purdue.edu/BTPFL (I. Mudawar).

0017-9310/$ - see front matter © 2013 Elsevier Ltd. All rights reserved.
http://dx.doi.org/10.1016/j.ijheatmasstransfer.2013.05.070

Nomenclature

A	cross-sectional area of flow channel
A_h	heated area of flow channel
A_w	area of wetting front
b	ratio of wetting front length to wavelength
Bo	Bond number
D_h	hydraulic diameter
Fr	Froude number
G	mass velocity
g	gravity
g_e	earth gravity
H	height of flow channel
H_f	mean thickness of liquid layer
h_{fg}	latent heat of vaporization
H_g	mean thickness of vapor layer
L	heated length
P	pressure
q''_m	critical heat flux
U_f	mean velocity of liquid layer
U_g	mean velocity of vapor layer
U_∞	rise velocity of slug bubble
We	Weber number
x_e	thermodynamic equilibrium quality
z	axial distance
z_0	axial location where vapor layer velocity just exceeds liquid layer velocity
z^*	axial location for determining vapor layer thickness and critical wavelength in Interfacial Lift-off Model

Greek symbols

δ	vapor layer thickness
θ	flow orientation angle
λ_c	critical wavelength
ρ	density
σ	surface tension

Subscripts

f	saturated liquid
g	saturated vapor
in	inlet to heated portion of flow channel.

direction as the liquid flow. This imparts flow stability to the system and helps achieve relative high CHF values by aiding vapor removal from, and liquid replenishment of the heated wall. This explains why the majority of published studies on flow boiling CHF are conducted in the vertical upflow orientation. While different mechanisms have been proposed for flow boiling CHF [21–25], photographic evidence points to a dominant *Wavy Vapor Layer Regime* commencing along the heated wall as CHF is approached, and CHF being triggered by an *Interfacial Lift-off Mechanism* [26–31], which will be discussed later.

Flow boiling CHF for all other orientations can be highly complicated by the manner in which buoyancy influences the vapor and liquid flows both along the flow channel and perpendicular to the heated wall. Fig. 1(a) is used as a guide to explain the influence of flow orientation on CHF for a flow channel that is heated along one side. Shown are eight channel flow orientations, with the flow radiating outwards, and the placement of the heated wall, indicated by a black rectangular strip.

1.4. Influence of buoyancy along the flow channel

The influence of buoyancy *along* the channel is especially problematic for vertical downflow, $\theta = 270°$. Here, buoyancy opposes the liquid forces – both drag and shear – and flow behavior is therefore a function of the relative magnitude of buoyancy and liquid forces. Zhang et al. [28,29] showed that the vertical downflow orientation results in one of three possible CHF regimes. At very low flow rates, buoyancy exceeds liquid forces, causing the vapor to flow backwards (vertically upwards) along the channel with CHF associated with a *Vapor Counterflow Regime* and *Flooding* and CHF values are quite small. Increasing the flow rate increases the relative magnitude of the liquid forces, and a particular flow rate is reached that causes a balance between the two opposing forces, causing the vapor to stagnate along the channel. Here, CHF is associated with a *Stagnation Regime*, and corresponding CHF values are vanishingly small. A further increase in flow rate causes the liquid forces to exceed buoyancy, and the vapor to flow concurrently with the liquid. CHF for these conditions is associated with a *Separated Concurrent Vapor Flow Regime*, and CHF values are appreciably greater than those for the *Vapor Counterflow* or *Stagnation Regimes*. In the limit of a very high flow rate, the liquid forces render any buoyancy effects negligible, and CHF values for vertical upflow and vertical downflow converge. Clearly, high flow rate is an effective means to negating the influence of buoyancy on both flow behavior along the channel and CHF magnitude.

1.5. Influence of buoyancy perpendicular to the heated wall

The influence of buoyancy perpendicular to the heated wall is most noticeable for horizontal flow orientations with the heated wall pointing upwards, $\theta = 0°$, and downwards, $\theta = 180°$ [28,29]. For $\theta = 0°$ and small flow rates, small bubbles that nucleate along the heated wall tend to coalesce together to form larger vapor bubbles, which are driven by buoyancy across the channel to the opposite adiabatic wall. Here, CHF is associated with a *Pool Boiling Regime*. For $\theta = 180°$ and small flow rates, buoyancy causes the vapor to stratify above the liquid and adjacent to the heated wall. Clearly, this *Stratification Regime* impedes liquid access to the heated wall, resulting in very low CHF values. By greatly increasing the flow rate for both horizontal orientations, the flow behavior at CHF begins to resemble that for vertical upflow, $\theta = 90°$. Furthermore, CHF values for $\theta = 0°$ and $180°$ at high flow rates converge with those for vertical upflow, $\theta = 90°$. The convergence of CHF values for different orientations at high flow rates has been confirmed in several prior studies [32–35].

1.6. Importance of wavy layer regime

Fig. 1(b) shows CHF data for FC-72 measured by Zhang et al. [29] in a flow velocity–orientation plane. The data are grouped into the six aforementioned CHF regimes for which representative photographs are also depicted in Fig. 1(b). Notice that all CHF regimes other than the *Wavy Vapor Layer Regime* are encountered at low velocities, while the *Wavy Vapor Layer Regime* is dominant at high velocities regardless of orientation. Interestingly, the *Wavy Vapor Layer Regime* is prevalent in the vertical and near-vertical upflow orientations, $\theta = 90°$ and $135°$, respectively, even at low velocities.

In a subsequent study, Zhang et al. [36] performed similar flow boiling experiments in parabolic flight to simulate microgravity. In the absence of buoyancy, the *Wavy Vapor Layer Regime* was

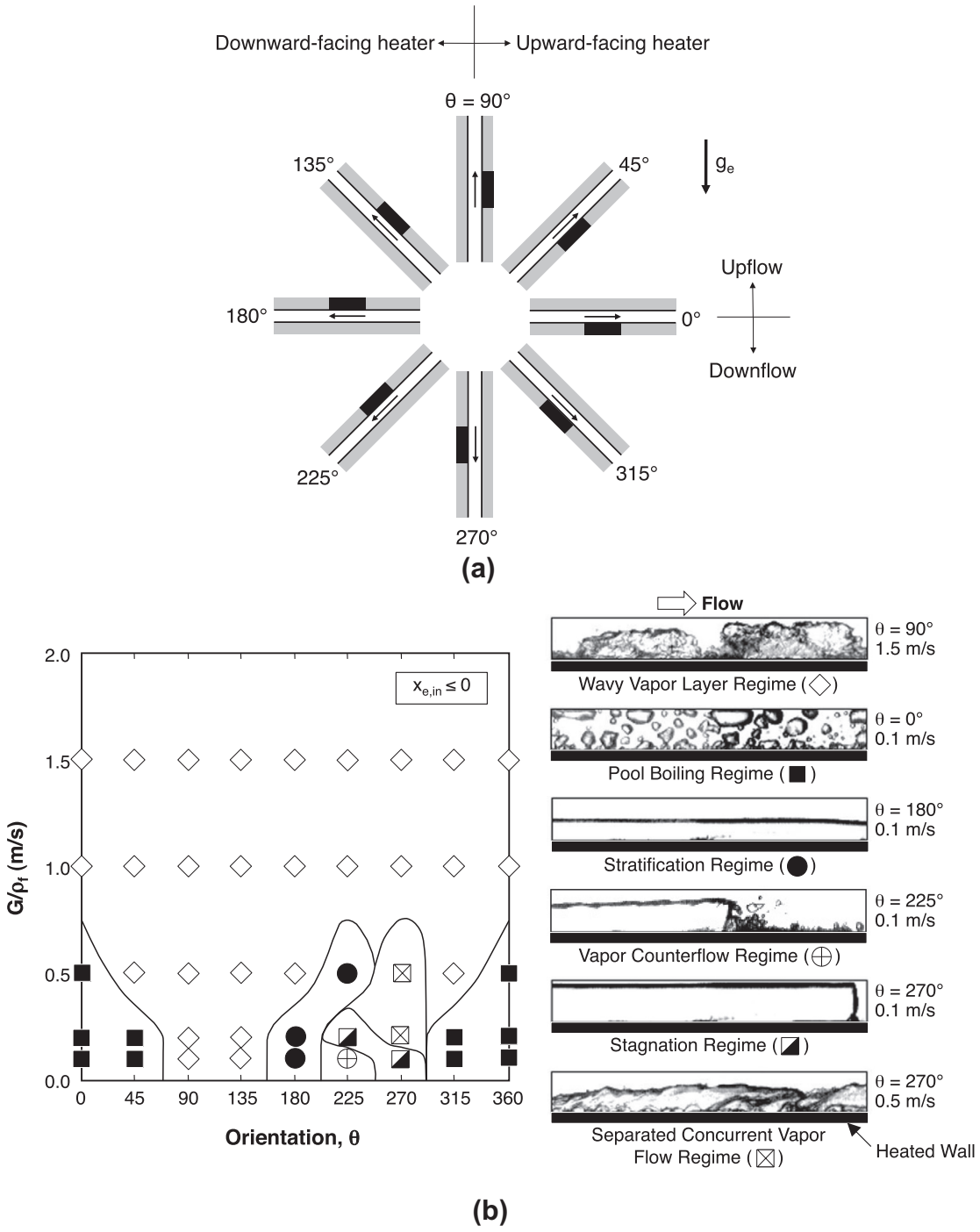

Fig. 1. (a) Flow orientation nomenclature (heated wall is indicated by a black rectangular strip). (b) CHF regime map for FC-72 and photos of representative CHF regimes. Adapted from Zhang et al. [29].

observed over the entire range of velocities, Fig. 2(a), including low velocities that resulted in the other more complex CHF regimes in 1 g_e experiments.

Interestingly, the *Wavy Vapor Layer Regime* has been observed at 1 g_e even in saturated pool boiling. While CHF for a horizontal upward-facing heated wall follows the classical depiction of Zuber et al. [3], tilting the wall to near vertical orientations resulted in a wavy vapor layer pattern [37,38] as shown in Fig. 2(b). The same behavior was observed in pool boiling along a downward-facing convex surface in 1 g_e [39] as shown in Fig. 2(c).

1.7. Threshold flow rate for flow boiling CHF

Clearly, increasing flow rate in channel flow boiling precipitates uniformity in interfacial behavior before CHF, with the *Wavy Vapor Layer Regime* occurring along the heated wall, and CHF triggered by the *Interfacial Lift-off Mechanism* regardless of orientation.

The discussion above concerns working fluid that is supplied to the channel in pure liquid state, *i.e.*, with $x_{e,in} \leqslant 0$. Recently, Kharangate et al. examined flow boiling CHF with the fluid entering the channel as a two-phase mixture ($x_{e,in} > 0$) in vertical upflow

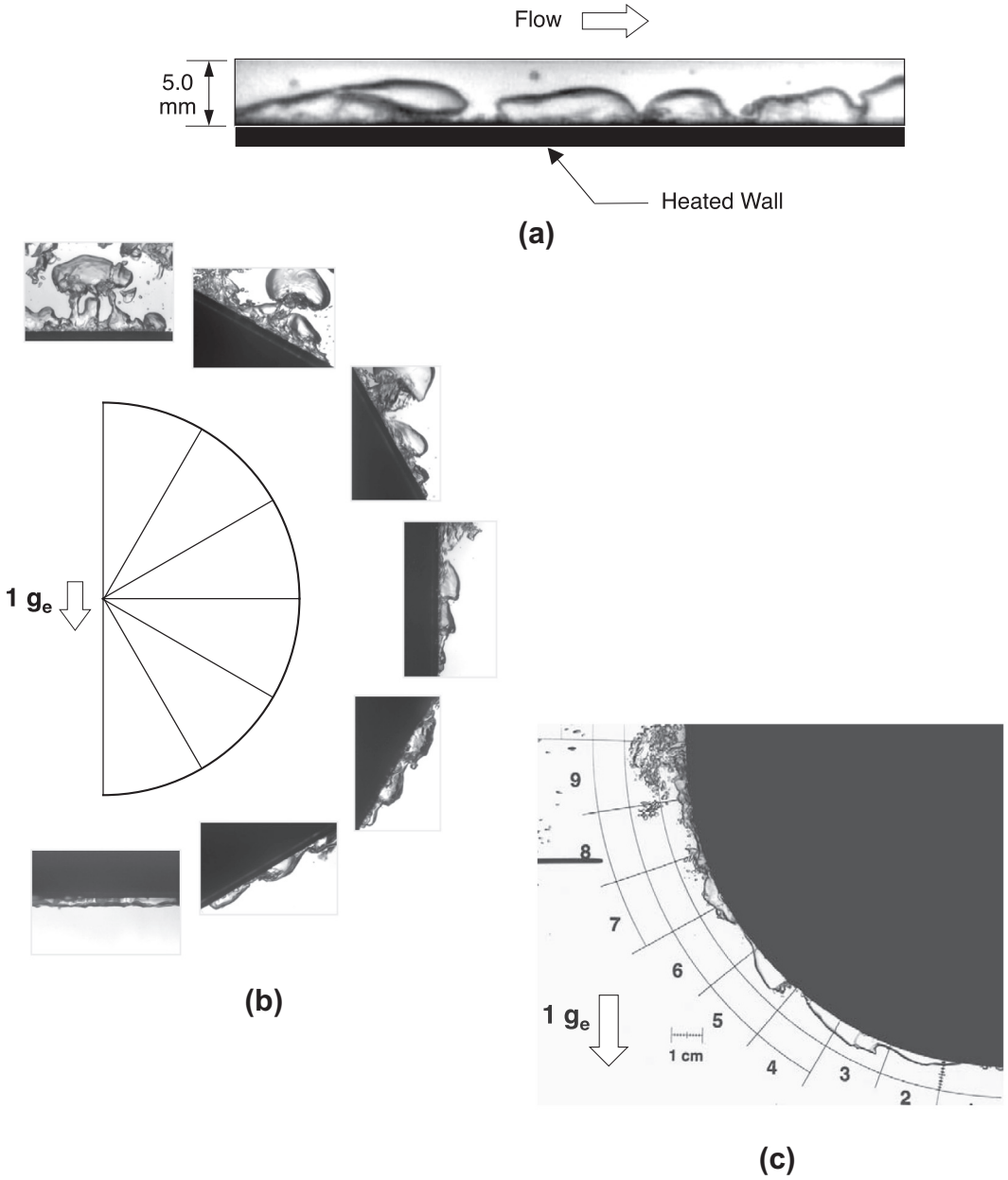

Fig. 2. Wavy vapor layer CHF regime for (a) flow boiling of FC-72 in microgravity at 0.25 m/s inlet velocity [36], (b) pool boiling of PF-5052 at different wall orientations at 1 g_e [37,38], and (c) pool boiling of FC-87 along a downward-facing convex wall at 1 g_e [39].

[40] and horizontal flow with the heated wall facing upwards [41]. Despite the complicated flow patterns caused by the incoming two-phase mixture, CHF for both orientations was predicted with good accuracy using the *Interfacial Lift-off Mechanism* employed by Zhang et al. for pure liquid inlet conditions ($x_{e,in} \leqslant 0$) in conjunction with the *Wavy Vapor Layer Regime* both at different flow orientations in 1 g_e[28,29] and in microgravity [36]. The authors of the present study extended the work of Kharangate et al. for all flow orientations [42]. They proved that, for two-phase mixture inlet conditions ($x_{e,in} > 0$), high flow rates cause appreciable diminution in the influence of orientation on CHF. This behavior was explained by the higher mass velocities increasing the magnitude of shear and drag forces compared to buoyancy, especially for high inlet qualities.

The studies by Zhang et al. [28,29,36], Kharangate et al. [40,41], and Konishi and Mudawar [42] all point to the existence of a threshold flow rate above which virtually identical CHF values are measured for all orientation. This threshold is of paramount importance to future space systems since, by operating the thermal management system at a flow rate that exceeds this threshold, one is able to utilize, with confidence, the vast body of published CHF data, correlations and models developed from ground-based studies for design of reduced gravity thermal management systems.

1.8. Objectives of study

The present study is part of a long-term collaborative study between the Purdue University Boiling and Two-Phase Flow Laboratory (PU-BTPFL) and the NASA-Glenn Research Center (NASA-GRC) to investigate the influence of gravity on both flow boiling and condensation. Studies are initiated by exploring the effects of flow orientation relative to Earth's gravity in ground experiments. The

same experiments are repeated in parabolic flight to simulate microgravity. Findings from both operating environments are used to assist the design of test hardware for future experiments onboard the International Space Station (ISS). The present study addresses flow boiling CHF in ground-based $1-g_e$ experiments.

The present study is focused on flow boiling CHF corresponding to different orientations with two-phase mixture inlet conditions ($x_{e,in} > 0$). Saturated inlet conditions are of great practical importance to thermal management of space systems, where a number of heat dissipating electronic or power sources are cooled in series. With this arrangement, the upstream modules can take advantage of subcooled flow boiling, while the downstream sources may be exposed to a two-phase mixture. This study, which is a follow-up to [42], will discuss extensive video records of flow boiling CHF that were captured at different flow rates, inlet qualities and flow orientations. A combination of video results, CHF data, and theoretical models is used to develop systematic criteria for assessing the influence of gravity on flow boiling CHF and, more specifically, for negating the influence of gravity altogether.

2. Experimental methods

2.1. Flow loop and flow boiling module

A closed two-phase flow loop was constructed to deliver FC-72 to a flow boiling test module at the desired pressure, mass velocity and quality. As shown in Fig. 3(a), FC-72 liquid is pumped from a reservoir into a filter, a turbine flow meter, and two in-line electric heaters before entering the flow boiling test module as a two-phase mixture. The two-phase mixture exiting the flow boiling module is routed through an air-cooled heat exchanger to return the fluid to liquid state. Pressure control for the loop is achieved with the aid of a nitrogen-filled accumulator situated between the heat exchanger and the reservoir.

To rid the working fluid from non-condensable gases prior to testing, a careful deaeration procedure is performed that consists of vigorous boiling, using an immersion heater internal to the reservoir, and condensation, via a water-cooled coil located near the top of the reservoir, while allowing non-condensable gases to exit freely to the ambient.

Fig. 3(b) shows the entire loop, in addition to power control and instrumentation cabinets, mounted onto a single rigid frame constructed from extruded aluminum members.

The flow boiling test module is designed to conduct flow boiling CHF measurements and allow video motion analysis of the two-phase flow along a uniformly heated wall. It consists of two transparent plastic (Lexan) plates that are bolted together, trapping a Teflon cord to ensure leak-proof assembly. As shown in Fig. 3(c), a 5.0-mm high by 2.5-mm wide flow channel is milled into the top plastic plate. The flow boiling module features an inlet plenum fitted with a flow straightening honeycomb insert to break up inlet eddies. The flow channel consists of three sections, an upstream adiabatic section for flow development, a 101.6-mm long section containing a heated copper plate affixed to the channel's bottom wall, and a downstream adiabatic section leading to the exit plenum. Rotation of the flow boiling module is achieved with the aid of a 0–360° swivel.

Six 4.0-mm wide and 16.1-mm long thick-film resistors are used to heat the copper plate as illustrated in Fig. 3(d). The resistors are soldered to the underside of the copper plate and connected in parallel to a 115-VAC variac. The copper wall temperature is measured by five type-K thermocouples inserted into small holes between the resistors.

Two-phase flow behavior along the channel is captured with the aid of a Photron Fastcam Ultima APX camera system with a shutter speed of 1/20,000 s. Video capture is achieved at a frame rate of 4000 fps, and high magnification made possible with the aid of a Nikon Micro-Nikkor 105 mm f/8D autofocus lens. As shown in Fig. 3(e), the camera is positioned normal to one side of the transparent flow-channel, and video imaging is performed at the inlet, middle, and exit portions of the heated portion of the channel.

2.2. Operating conditions and measurement accuracy

The test conditions for this study include mass velocities corresponding to $G/\rho_f = 0.126$–1.130 m/s, inlet qualities of $x_{e,in} = 0.01$–0.19, and all eight orientations depicted in Fig. 1(a), with the pressure at the outlet from the heated wall maintained constant at 103 kPa (15 psia).

As indicated in [36], the accuracy of pressure transducer measurements upstream and downstream of the heated wall, and temperature measurements along the heated wall and at various locations along the flow loop are estimated at 0.01% and 0.3 °C, respectively. The uncertainty in the heat flux measurement is 0.2%.

3. CHF regimes

3.1. CHF regimes at low mass velocity ($G/\rho_f = 0.224$ m/s and $x_{e,in} = 0.01$)

At low mass velocities, CHF values are generally low and buoyancy results in complex boiling regimes. The subcooled CHF regime map, Fig. 1(b), will serve as a guideline to identify any similarities or differences in CHF behavior for the present study corresponding to $x_{e,in} > 0$ with the CHF behavior captured by Zhang et al. [29] for $x_{e,in} \leqslant 0$. Fig. 4(a)–(h) show the vapor development at the inlet and middle regions at CHF- (just prior to CHF) for all orientations at $G/p_f = 0.224$ m/s and $x_{e,in} = 0.01$. For each orientation in Fig. 4, fifteen sequential video frames are presented for each of the inlet and middle regions; the time elapsed between consecutive frames is 0.0006 s. Zhang et al. [29] identified a *Pool Boiling Regime* for all upward-facing heated wall orientations ($\theta = 0°$, 45° and 315°) at low mass velocities with $x_{e,in} \leqslant 0$. For the present study, corresponding to $x_{e,in} > 0$, the flow for the upward-facing heated wall orientations enters the heated portion of the channel fully separated, with a liquid layer covering the heated wall and a thick vapor layer residing atop. For $\theta = 0°$ and 315°, the *Pool Boiling Regime* is replaced by the *Wavy Vapor Layer Regime*, Fig. 4(a), as a thick wavy vapor layer begins to form along the heated wall beneath the liquid layer. Interestingly, Zhang et al. encountered the *Wavy Vapor Layer Regime* at $\theta = 0°$ and 315° only at high mass velocities. This difference in CHF- behavior can be explained by the finite inlet void fraction in the present study producing higher flow velocities and higher shear stresses. The liquid layer adjacent to the heated wall is now sandwiched between the central vapor core and newly developed wavy vapor layer, and breaks apart in the middle region in the form of liquid ligaments, which provide partial wetting of the heated wall downstream.

The *Pool Boiling Regime* is encountered in the present study only at $\theta = 45°$ as depicted in Fig. 4(b) for the inlet region. Here too, the flow enters the heated portion of the channel fully separated, with the heated wall covered with a liquid layer beneath a thick vapor layer. Because of the relatively low liquid velocity, bubbles that nucleate along the heated wall are removed by buoyancy towards the vapor–liquid interface where they are released into the vapor layer. Farther downstream in the middle region, the increased void fraction increases the velocities of the liquid and vapor layers, causing vapor bubbles to coalesce along the heated wall into a fairly continuous wavy vapor layer beneath the liquid layer. The

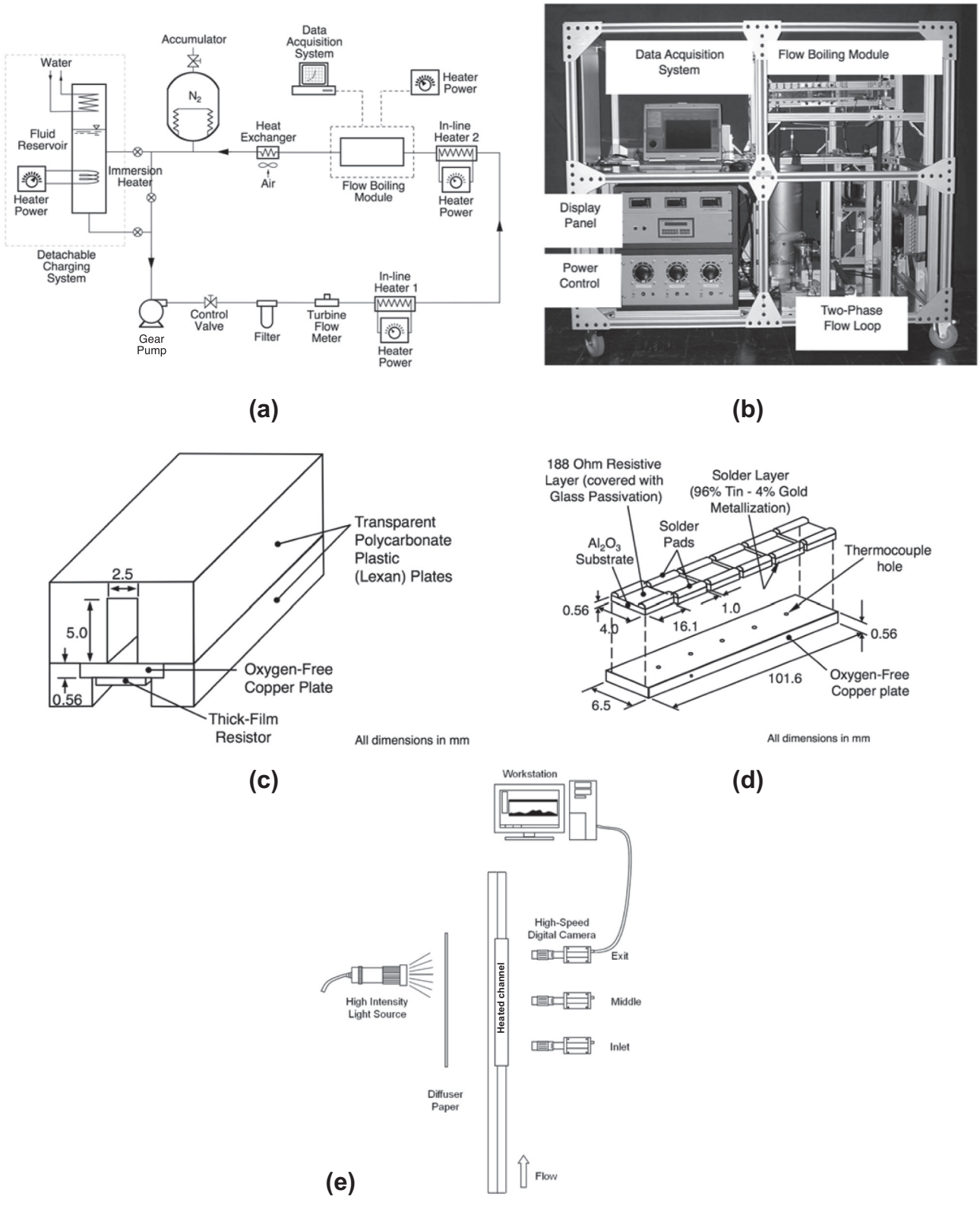

Fig. 3. (a) Schematic of two-phase flow loop. (b) Photo of test facility. (c) Construction of the flow channel. (d) Construction of the heated wall. (e) Inlet, middle and exit regions of the heated portion of the flow channel used for video capture.

liquid layer is now sandwiched between the heated wall vapor layer and the vapor layer above. The liquid layer is gradually consumed in the flow direction, with ligaments occasionally breaking off and providing wetting for the heated wall downstream.

Fig. 4(c) shows the interfacial behavior at CHF- for vertical upflow, $\theta = 90°$. Here, the flow entering the heated portion of the channel consists of a liquid layer covering all four channel walls, surrounding a central vapor core. At CHF-, vapor is generated

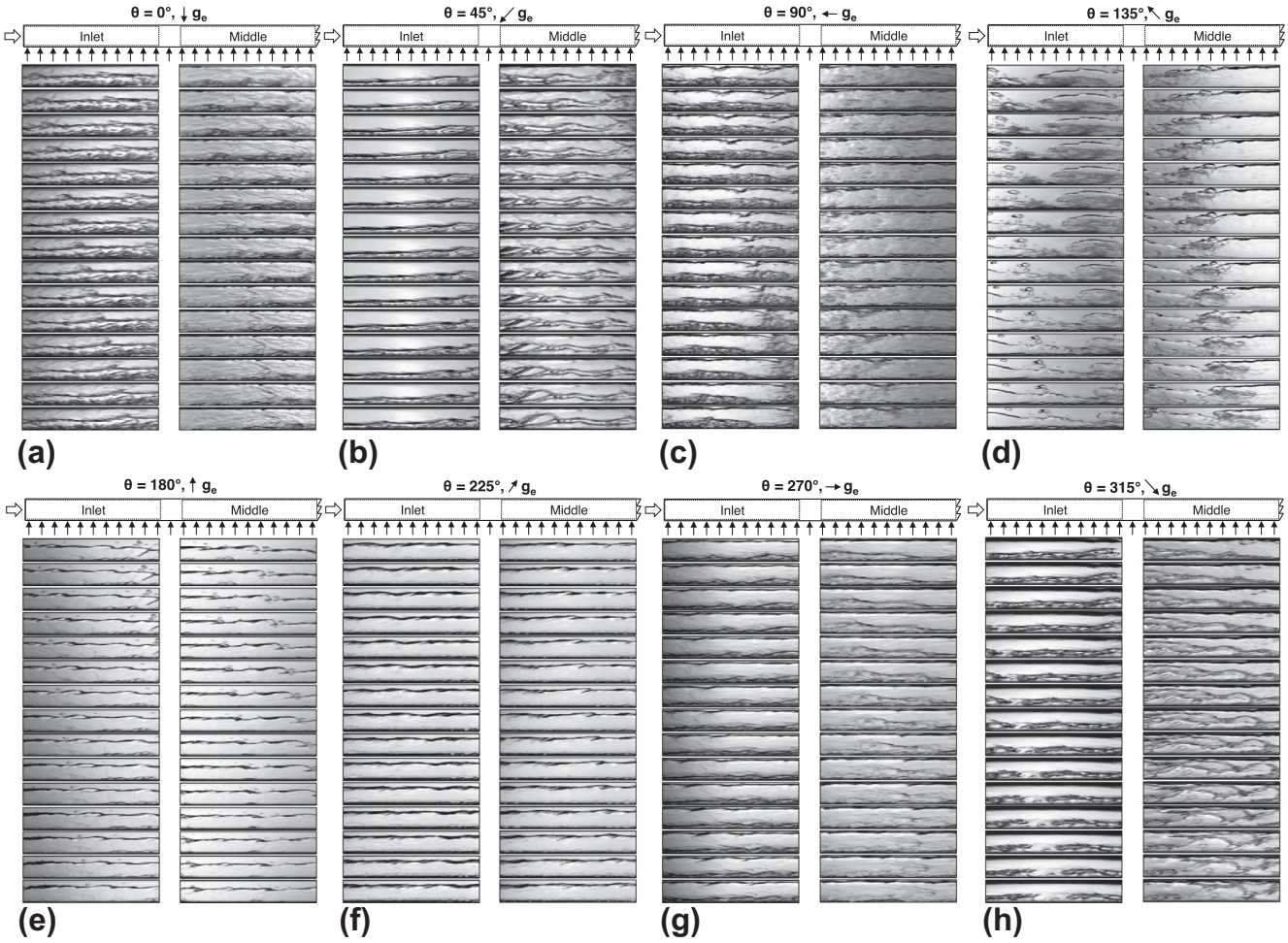

Fig. 4. Sequential images of two-phase flow in inlet and middle regions of heated wall captured at CHF- for $G/\rho_f = 0.224$ m/s and $x_{e,in} = 0.01$ for (a) $\theta = 0°$, (b) $\theta = 45°$, (c) $\theta = 90°$, (d) $\theta = 135°$, (e) $\theta = 180°$, (f) $\theta = 225°$, (g) $\theta = 270°$, and (h) $\theta = 315°$.

within the liquid layer in contact with the heated wall, causing separation of the liquid layer in the inlet region. The vapor layer also persists along the heated wall in the middle region. This behavior is reminiscent of the *Wavy Vapor Layer Regime* identified by Zhang et al. [29] for $\theta = 90°$ and $x_{e,in} \leqslant 0$. Farther downstream, the separated liquid layer adjacent to the heated wall suffers appreciable thinning due to an axial increase in shear stresses brought upon by the axial acceleration associated with phase change.

Fig. 4(d) shows sequential images for CHF- at $\theta = 135°$. Here, the flow enters the heated portion of the channel with vapor stratified against the heated wall, and liquid flowing against the opposite insulated wall at low velocity. This behavior is characteristic of the *Stratification Regime*. But unlike the other stratified regimes corresponding to $\theta = 180°$ and 225°, CHF- at $\theta = 135°$ is associated with appreciable interfacial waviness. With the liquid separated from the heated wall, this orientation yields a low CHF of only 8.90 W/cm^2.

For the horizontal downward-facing heated wall orientation, $\theta = 180°$, and downflow with a downward-facing heated wall, $\theta = 225°$, CHF- at $G/p_f = 0.224$ m/s and $x_{e,in} = 0.01$ follows a clear *Stratification Regime* as depicted in Fig. 4(e) and (f), respectively. Here, the flow is well separated, with a vapor layer stratified along the heated wall, preventing the liquid beneath to access the heated wall. This behavior results in low CHF values and the stratified vapor layer is initiated immediately at the inlet. Relatively small velocity differences between the liquid and vapor layers impart stability to the liquid–vapor interface, ensuring clear separation and stratification of the vapor layer, and limited access of liquid to the heated wall. Interestingly, the behavior depicted in Fig. 4(f) for $\theta = 225°$ yields an unusually small CHF of only 1.85 W/cm^2.

Fig. 4(g) shows CHF- behavior for vertical downflow, $\theta = 270°$. Like vertical upflow, $\theta = 90°$, the flow entering the channel at $\theta = 270°$ is comprised of a liquid layer that covers all four channel walls surrounding a central vapor core. Vapor production within the liquid layer in contact with the heated wall causes separation of the liquid layer in the inlet region, which is consistent with the *Wavy Vapor Layer Regime*. While this CHF- behavior may appear to resemble that observed at $\theta = 90°$, there are appreciable differences between the two orientations, with the buoyancy aiding the vapor removal for $\theta = 90°$ and resisting the flow for $\theta = 270°$. This difference is manifest in the middle region where a much thicker vapor layer for $\theta = 270°$ contributes to more significant wall dryout. It should be noted here that Zhang et al. [29] identified three distinct CHF regimes for $x_{e,in} \leqslant 0$ at $\theta = 270°$: (i) *Vapor Counterflow Regime* at very low mass velocities, where buoyancy exceeds liquid forces, (ii) *Stagnation Regime,* where the two forces are equal, and (iii) *Separated Concurrent Vapor Flow Regime*, where liquid forces exceed buoyancy. Interestingly, the *Vapor Counterflow Regime* and *Stagnation Regime* were never observed in the present study corresponding to $x_{e,in} > 0$. This is apparently the result of

the greatly increased flow velocities when the flow enters the channel as a two-phase mixture.

Fig. 5 provides additional details concerning CHF- at $\theta = 135°$ for a very low mass velocity of $G/\rho_f = 0.126$ m/s and $x_{e,in} = 0.01$. Here, the flow enters the channel with vapor stratified against the heated wall in accordance with the *Stratification Regime*, with liquid flowing against the opposite insulated wall at very low velocity. The large velocity difference between the vapor and liquid renders the interface highly unstable in the middle region, where the interfacial amplitude increases greatly and the interfacial waves cause liquid droplets and ligaments to be deposited onto the heated wall. Interestingly, this liquid replenishment mechanism caused this orientation to produce the highest CHF of all the downward-facing heated wall orientations for $G/\rho_f = 0.126$ m/s.

3.2. CHF regimes at intermediate mass velocity ($G/\rho_f = 0.398$ m/s and $x_{e,in} = 0.01$)

Fig. 6(a)–(h) show sequential images for all orientations at $G/\rho_f = 0.398$ m/s and $x_{e,in} = 0.01$. Because of the relatively high mass velocity, there is greater interfacial instability for all upward-facing heated wall orientations of $\theta = 315°$, 0°, and 45°, and better replenishment of the heated wall by liquid ligaments downstream, and therefore higher CHF than those corresponding to $G/\rho_f = 0.224$ m/s and $x_{e,in} = 0.01$. CHF- for these orientations is consistent with the *Wavy Vapor Layer Regime.* For vertical upflow, $\theta = 90°$, CHF- is associated with the *Wavy Vapor Layer Regime,* similar to that observed for $G/\rho_f = 0.224$ m/s and $x_{e,in} = 0.01$. Interestingly, this behavior is also prevalent at $G/\rho_f = 0.398$ m/s for all downward-

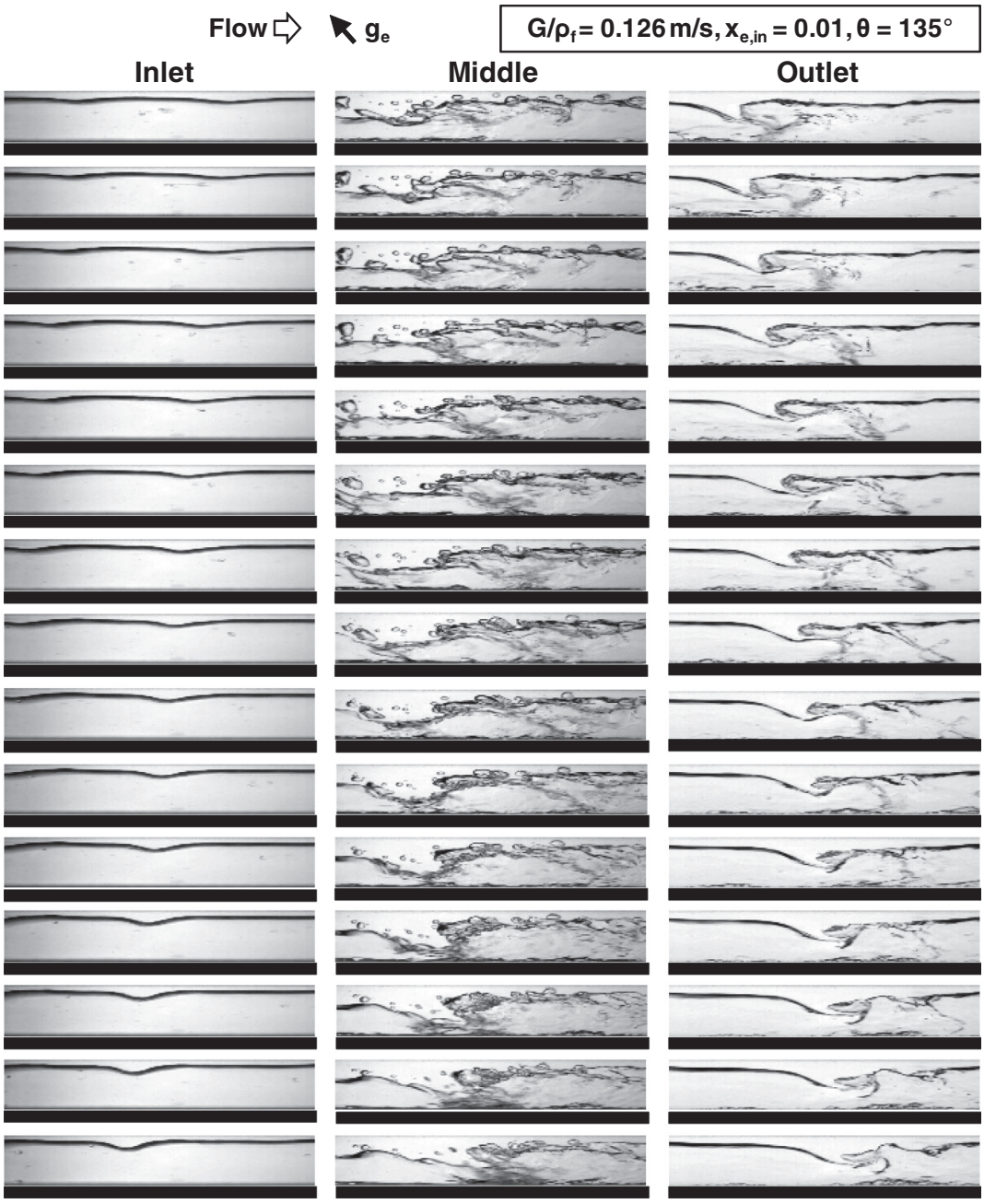

Fig. 5. Sequential images of inlet, middle, and outlet regions depicting *Stratification Regime* with interfacial waves observed at CHF- for $\theta = 135°$, $G/\rho_f = 0.126$ m/s and $x_{e,in} = 0.01$. The heated wall is indicated by a rectangular black strip.

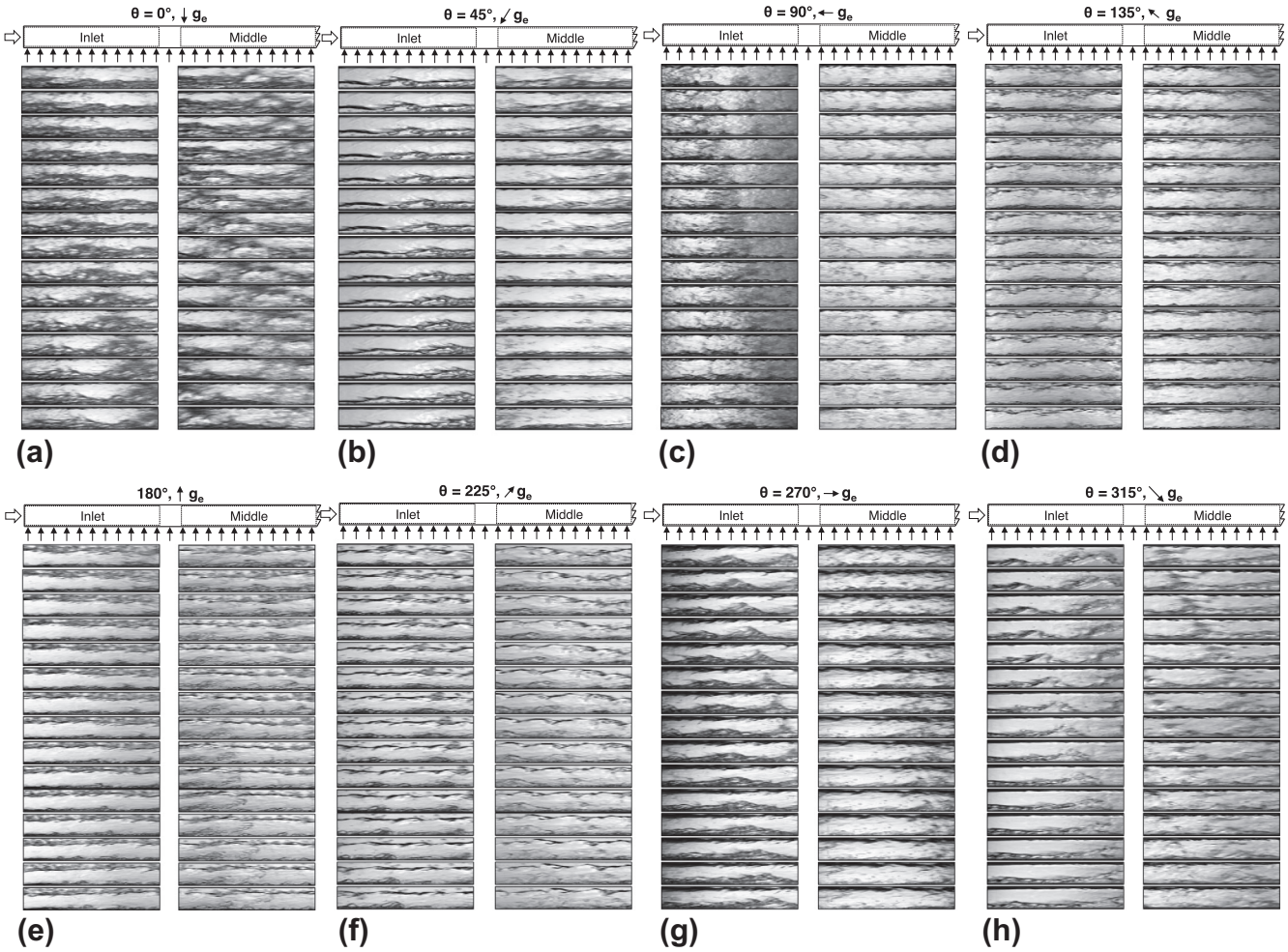

Fig. 6. Sequential images of two-phase flow in inlet and middle regions of heated wall captured at CHF- for G/ρ_f = 0.398 m/s and $x_{e,in}$ = 0.01 for (a) θ = 0°, (b) θ = 45°, (c) θ = 90°, (d) θ = 135°, (e) θ = 180°, (f) θ = 225°, (g) θ = 270°, and (h) θ = 315°.

facing heated wall orientations (θ = 135°, 180° and 225°), as well as for vertical downflow (θ = 270°). These findings prove that increasing mass velocity imparts uniformity in CHF mechanism regardless of orientation.

3.3. Summary of CHF regimes for different orientations

Fig. 7(a) and (b) show schematic representations of CHF- for G/p_f = 0.224 and 0.398 m/s, respectively, at $x_{e,in}$ = 0.01, corresponding to 90° orientation increments. Shown are both the longitudinal development of interfacial behavior as well as depictions of the cross-section both upstream and downstream of the heated portion of the channel.

For the lower mass velocity of G/p_f = 0.224 m/s, Fig. 7(a) shows the flow at θ = 0° enters the heated portion of the channel fully stratified, with the liquid covering the heated wall and the vapor flowing above. At CHF-, intense vapor effusion at the heated wall separates the liquid layer. For vertical upflow, θ = 90°, the flow enters the heated portion of the channel with a thin liquid layer covering all four channel walls, surrounding a large central vapor core. At CHF-, vapor effusion separates the liquid layer adjacent to the heated wall, but unlike θ = 0°, a thin liquid film continues to cover the three insulated walls of the channel. For horizontal flow with a downward-facing heated wall, θ = 180°, the flow enters the heated portion of the channel stratified with the vapor covering the heated wall. The heated wall receives minor cooling from liquid ligaments and droplets that are broken off the liquid layer but, because of the limited access of liquid to the heated wall, CHF is quite small for this orientation. For the vertical downward-facing orientation, θ = 270°, the flow enters the heated portion of the channel separated, with a liquid layer covering all four walls, surrounding a central vapor core, and CHF occurs when the vapor effusion separates the liquid layer adjacent to the heated wall. Overall, the interfacial behavior seems quite similar for θ = 90° and θ = 270°. However, CHF for the later is much smaller because buoyancy for this orientation opposes the liquid flow.

Fig. 7(b) shows schematic representations of CHF- at G/p_f = 0.398 m/s and $x_{e,in}$ = 0.01. Here, interfacial behavior is similar for all orientations and consistent with the *Wavy Vapor Layer Regime*, proving that high mass velocity is an effective means for overcoming the influence of orientation.

3.4. CHF regime maps

Fig. 8(a) and (b) summarize all CHF- regimes for $x_{e,in}$ = 0.01 in a mass velocity – orientation plane for the inlet and outlet regions, respectively. Shown in Fig. 8(a) are three clearly identifiable CHF-regimes for the inlet region, with the *Pool Boiling Regime* prevailing for the two lowest mass velocities at θ = 45°, the *Stratification Regime* for the lowest mass velocity at θ = 135°, 180° and 225°, and the *Wavy Vapor Layer Regime* for all other mass velocities and orientations. Fig. 8(b) shows, for the outlet region, the *Stratification*

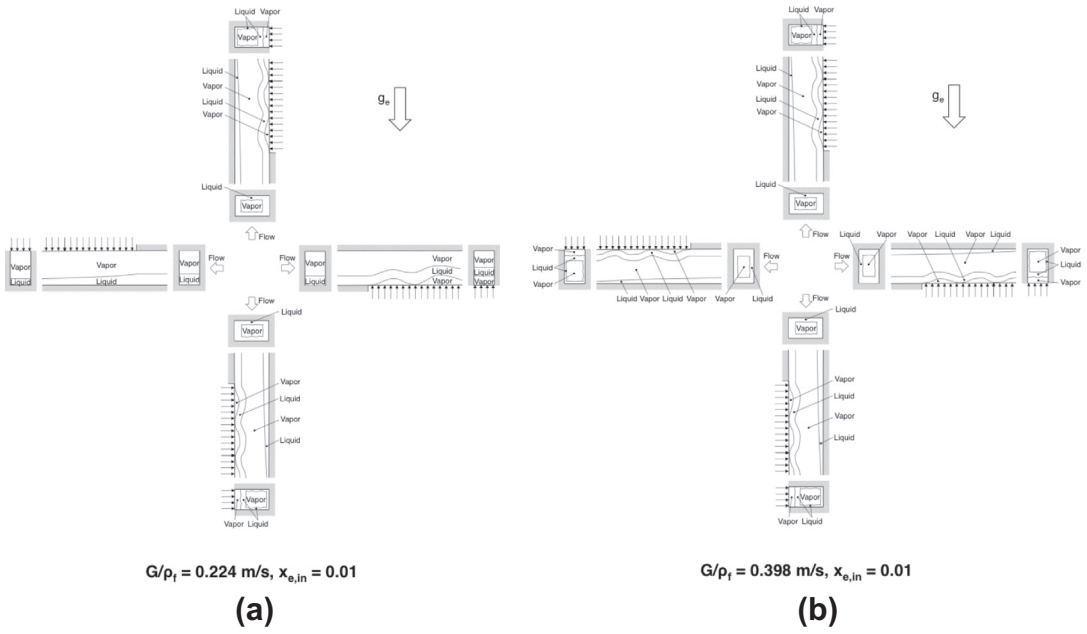

Fig. 7. Schematic representation of interfacial behavior at CHF- for different flow orientations for (a) $G/\rho_f = 0.224$ m/s and $x_{e,in} = 0.01$, and (b) $G/\rho_f = 0.398$ m/s and $x_{e,in} = 0.01$. Adapted from Konishi and Mudawar [42].

Regime prevailing for the same orientations as the inlet region and lowest mass velocity, and the *Wavy Vapor Layer Regime* for all other mass velocities and orientations. Overall, Fig. 8(a) and (b) show that all regimes other than the *Wavy Vapor layer Regime* are encountered in downward-facing heated wall orientations and at low mass velocities, where the influence of buoyancy is most pronounced.

Comparing the present CHF- regime maps for $x_{e,in} = 0.01$, Fig. 8(a) and (b), with those of Zhang et al. [29] for $x_{e,in} \leqslant 0$, Fig. 1(b), shows that $x_{e,in} > 0$ offers greater resistance to buoyancy, evidenced by a transition to the *Wavy Vapor Layer Regime* at lower mass velocities.

4. CHF results

4.1. CHF trends

Fig. 9(a) and (b) show CHF variations with orientation for $x_{e,in} = 0.01$ and 0.19, respectively, for different mass velocities. There are obvious similarities in these variations for different values of G/ρ_f and $x_{e,in}$, with higher CHF values achieved for upward-facing heated wall orientations ($\theta = 315°$, 0°, and 45°) and low values for downward-facing heated wall orientations ($\theta = 135°$, 180° and 225°). These trends are consistent in trend with those of Zhang et al. [28,29] for $x_{e,in} \leqslant 0$. Another obvious trend for each $x_{e,in}$ is the significant variation in CHF for low compared to high G/ρ_f. For example, the data in Fig. 9(a) corresponding to the two lowest mass velocities of $G/\rho_f = 0.126$ and 0.224 m/s, show appreciable reduction in CHF for several orientations. For all downward-facing heated wall orientations ($\theta = 135°$, 180° and 225°), weak inertia at the two lowest mass velocities allows buoyancy to stratify the vapor along the heated wall, resulting in very low CHF values. CHF is also low for vertical downflow ($\theta = 270°$), where buoyancy causes the vapor flow to impede that of the liquid, and compromises liquid replenishment of the wall. The trends in Fig. 9(b) for $x_{e,in} = 0.19$ are similar to those for $x_{e,in} = 0.01$, with higher CHF values achieved for upward-facing heated wall orientations ($\theta = 315°$, 0°, and 45°) and low values for downward-facing heated wall orientations ($\theta = 135°$, 180° and 225°. However, CHF values are higher for the higher inlet quality. Notice also that the influence of orientation on CHF for $G/\rho_f = 0.398$ m/s is greatly reduced for $x_{e,in} = 0.19$ compared to $x_{e,in} = 0.01$. These trends point to increasing mass velocity and inlet quality as two very effective means at combating the influence of buoyancy on flow boiling CHF.

4.2. Interfacial Lift-off Model

Hydrodynamic instability of the liquid–vapor interface at CHF- in accordance with the *Wavy Vapor Layer Regime* has been successfully modeled by a combination of three sub-models: (i) a separated flow control volume model that is used to determine the mean velocities of the vapor and liquid layers and thickness of the vapor layer generated along the heat wall, (ii) a hydrodynamic instability model that is employed to determine the wavelength of the vapor–liquid interface, and (iii) an *Interfacial Lift-off Criterion* as a trigger mechanism for CHF as shown in Fig. 10[42].

The *Interfacial Lift-off Criterion* is based on the observation that the wavy vapor layer generated at CHF- causes dryout over much of the heated wall save for *wetting fronts* corresponding to the wave troughs, where the liquid is able to reach the wall. Liquid contact with the wall is maintained by a pressure force associated with interfacial curvature in the wetting fronts. CHF is postulated to occur when the momentum of vapor in the wetting fronts perpendicular to the heated wall just exceed the pressure force, causing the interface to be lifted from the heated wall and precluding any further liquid contact with the wall.

This model has been very effective at predicting flow boiling CHF for both $x_{e,in} \leqslant 0$ [26–31,34–36] and $x_{e,in} > 0$ [40,41]. A recent study by the authors [42] provides details concerning all three sub-models that are used to predict flow boiling CHF for different orientations and $x_{e,in} > 0$. This model is used in the present study to determine flow conditions that cause the dominant *Wavy Vapor Layer Regime* observed at high mass velocities, especially for high $x_{e,in}$, to be replaced by the more complex, buoyancy dominated *Pool Boiling Regime* and *Stratification Regime*. Fig. 10(a) illustrates the CHF- flow pattern corresponding to the Wavy Vapor Layer Regime. The flow entering the heated portion of the channel consists of

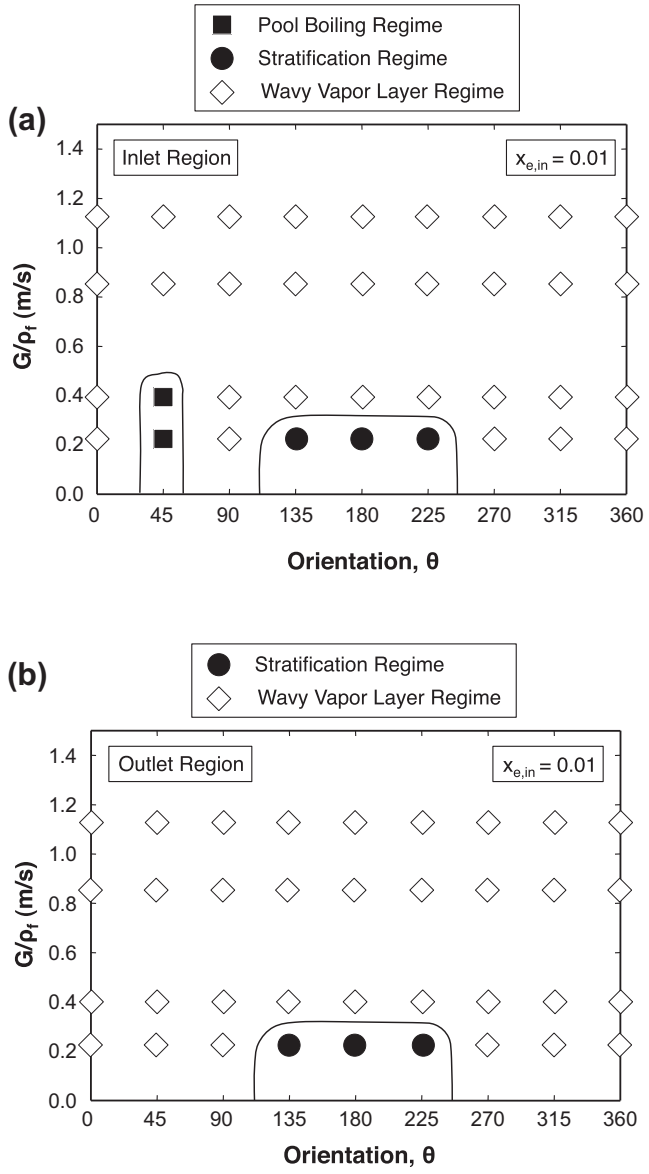

Fig. 8. CHF regime map for $x_{e,in} = 0.01$ for (a) inlet region and (b) outlet region.

liquid layers covering all four channel walls surrounding a central vapor core. A new vapor layer is generated along the heated wall at CHF- beneath the liquid layer adjacent to the heated wall. As discussed in [42], the separated flow model is used to determine (i) the mean thickness, H_f, and mean axial velocity, U_f, of liquid layer adjacent to the heated wall, and (ii) the mean thickness, H_g, and mean axial velocity, U_g, of the heated wall vapor layer. As discussed below, these parameters are used in the instability model to determine the critical wavelength, λ_c, and CHF is predicted according to the *Interfacial Lift-off Model* by the relation [42]

$$q''_m = \rho_g h_{fg}\left[\frac{4\pi\sigma b\sin(b\pi)}{\rho_g}\right]^{1/2}\left.\frac{\delta_g^{1/2}}{\lambda_c}\right|_{z^*}, \tag{1}$$

where $b = 0.2$ and $z^* = z_o + \lambda_c(z^*)$, where z_o is the distance from the leading edge of the heated wall to the location where the vapor velocity just overcomes the liquid velocity. It is assumed hydrodynamic instability generates the interfacial waves at z^*, where the wavy vapor layer begins to propagate along the heated wall. Both δ_g and λ_c are calculated at z^*.

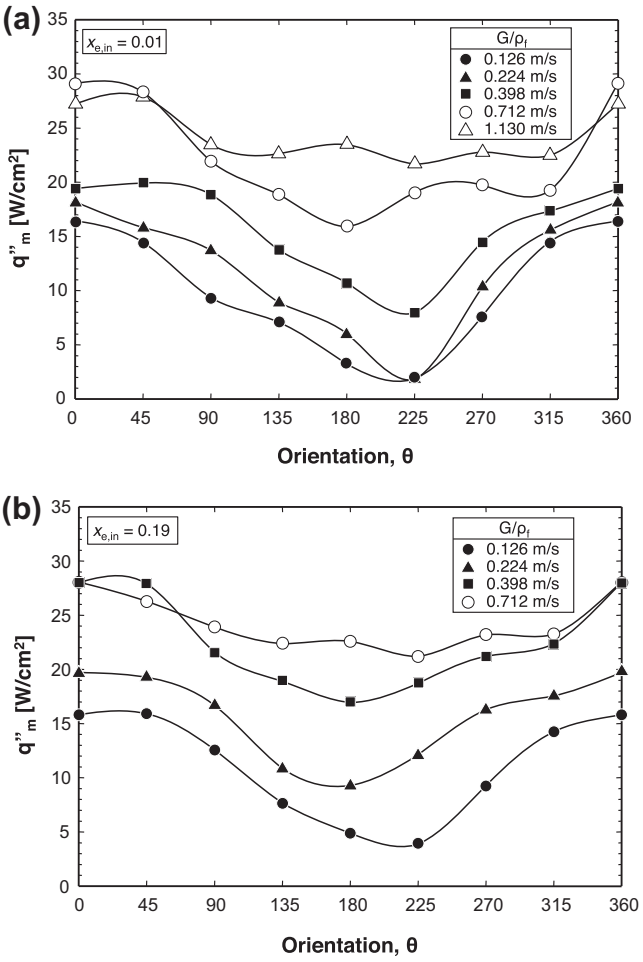

Fig. 9. Variation of CHF with flow orientation for different mass velocities at (a) $x_{e,in} = 0.01$ and (b) $x_{e,in} = 0.19$.

Fig. 11 shows the variation of measured CHF with orientation for the limiting mass velocities of $G/\rho_f = 0.126$ and 0.995 m/s and $x_{e,in} = 0.01$. Also shown for $G/\rho_f = 0.995$ m/s are CHF predictions based on the *Interfacial Lift-off Model*, which are in good agreement with the experimental data. For $G/\rho_f = 0.126$ m/s, Fig. 11 also shows predictions of the classical pool boiling model of Zuber et al. [3],

$$q''_m = 0.131\rho_g h_{fg}\left[\frac{\sigma(\rho_f-\rho_g)g_e\cos\theta}{\rho_g^2}\right]^{1/4}. \tag{2}$$

Fig. 11 includes predictions based on a relation by Nejat [43] for CHF resulting from flooding,

$$q''_m = 0.36\left(\frac{L}{D_h}\right)^{0.1}\left(\frac{A}{A_h}\right)\rho_g h_{fg}\left[\frac{(\rho_f-\rho_g)g_e D_h}{\rho_g}\right]^{1/2}\left[1+\left(\frac{\rho_g}{\rho_f}\right)^{1/4}\right]^{-2}, \tag{3}$$

where L, D_h, A, and A_h are the heated length, hydraulic diameter, channel cross-sectional area, and heated area, respectively. Notice how, for the low mass velocity, Zuber et al. model provides good predictions for horizontal and near-horizontal upward-facing heated wall orientations ($\theta = 315°$, 0° and 45°).

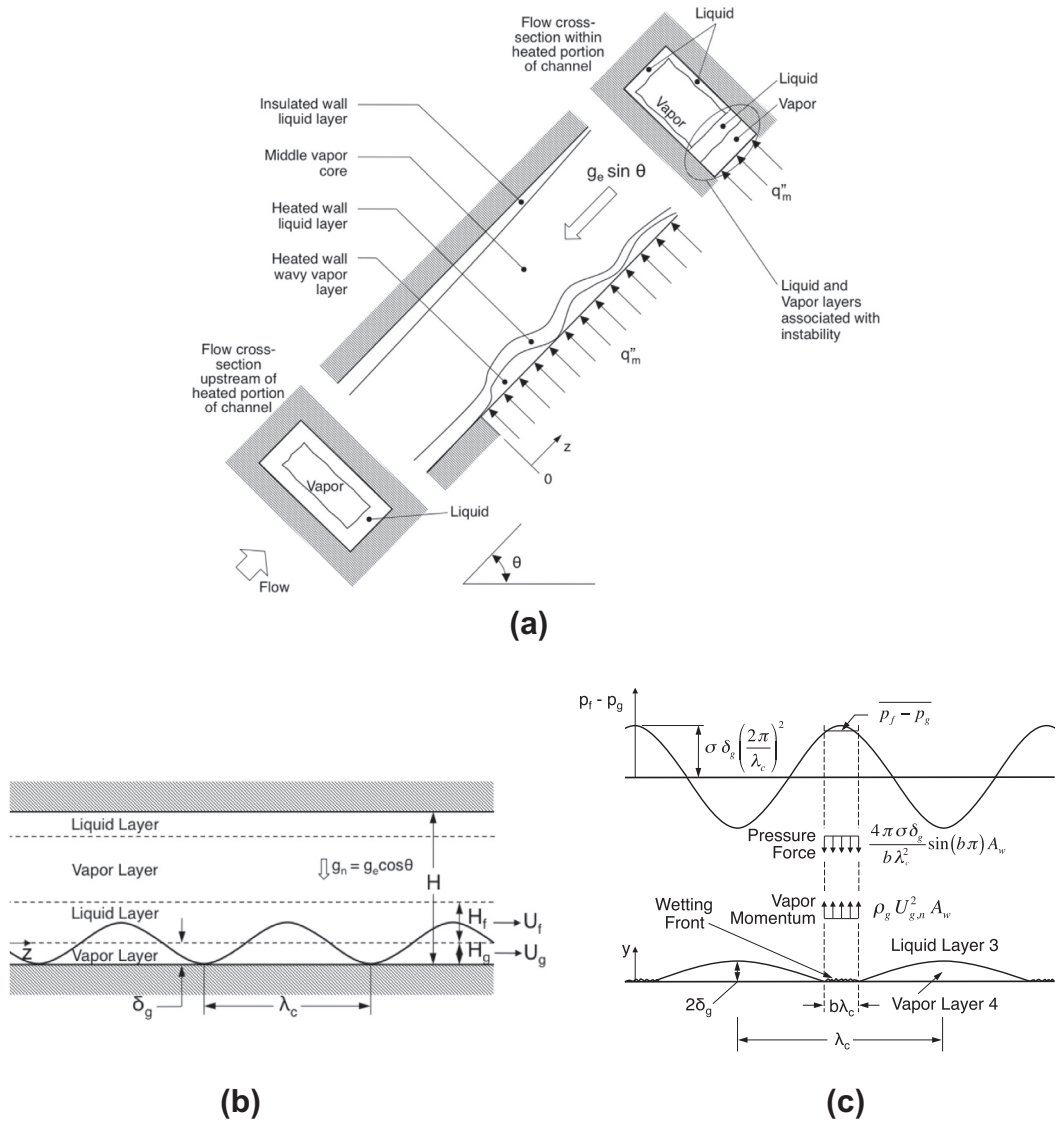

Fig. 10. (a) Schematic of separated layers at CHF- for high mass velocities. (b) idealized wavy vapor layer formation along heated wall at CHF-. (c) *Interfacial Lift-off Criterion* applied to wetting front.

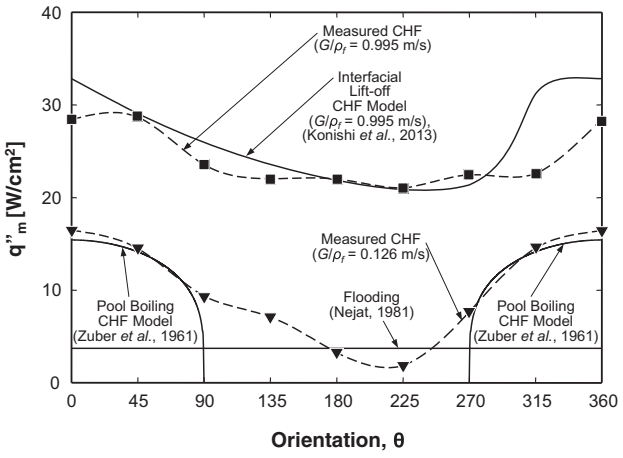

Fig. 11. Comparison of CHF data for lowest and highest mass velocities and $x_{e,in}$ = 0.01 with predictions based on previous models and correlations.

5. Criteria for overcoming influence of gravity on flow boiling CHF

5.1. Overall methodology

The method used to develop criteria for overcoming the effects of gravity on flow boiling CHF with $x_{e,in} > 0$ is based on the technique developed by Zhang et al. [29] for $x_{e,in} \leqslant 0$. The present criteria for $x_{e,in} > 0$ are complicated by the influence of inlet void fraction. Introduced below are criteria for:

(1) Overcoming the influence of gravity perpendicular to the heated wall based on hydrodynamic instability analysis of the vapor–liquid interface,
(2) Overcoming the influence of gravity opposite to the fluid flow. This gravity component governs vapor removal (or flooding for low mass velocities and downflow orientations) along the flow direction, and

(3) Ensuring that the wavelength of the liquid–vapor interface is smaller than the heated length to facilitate liquid contact with wall.

5.2. Criterion for negating influence of component of gravity perpendicular to heated wall

Classical instability theory are based on the assumption of a sinusoidal vapor–liquid interface. Potential flow relations coupled with appropriate velocity boundary conditions are imposed for each phase as well as along the interface in between [44,45]. Another interfacial boundary condition is that pressure difference due to the sinusoidal perturbation is balanced by surface tension. This method results in the following relation for the critical wavelength, λ_c, corresponding to a neutrally stable wave.

$$\frac{2\pi}{\lambda_c}\frac{\sigma(\rho_f+\rho_g)}{\rho_f\rho_g(U_g-U_f)^2}=\frac{1}{2}\left\{1+\sqrt{1+4\frac{(\rho_f-\rho_g)(\rho_f+\rho_g)^2\sigma g_e\cos\theta}{\rho_f^2\rho_g^2(U_g-U_f)^4}}\right\}. \quad (4)$$

Eq. (4) indicates that interfacial instability is governed by the combined influences of inertia, surface tension, and component of gravity that is perpendicular to the heated wall. Eq. (4) also reveals that the influence of gravity becomes negligible when

$$\left|\frac{(\rho_f-\rho_g)(\rho_f+\rho_g)^2\sigma g_e\cos\theta}{\rho_f^2\rho_g^2(U_g-U_f)^4}\right|\ll\frac{1}{4}, \quad (5)$$

which reduces Eq. (4) to

$$\lambda_c=\frac{2\pi\sigma(\rho_f+\rho_g)}{\rho_f\rho_g(U_g-U_f)^2}. \quad (6)$$

Eq. (5) can also be presented in terms of the Bond and Weber numbers,

$$\left|\frac{Bo}{We^2}\right|=\left|\frac{(\rho_f-\rho_g)(\rho_f+\rho_g)^2\sigma g_e\cos\theta}{\rho_f^2\rho_g^2(U_g-U_f)^4}\right|\ll\frac{1}{4}, \quad (7)$$

$$\text{where}\quad Bo=\frac{(\rho_f-\rho_g)g_e\cos\theta L^2}{\sigma} \quad (8)$$

$$\text{and}\quad We=\frac{\rho_f\rho_g(U_g-U_f)^2L}{(\rho_f+\rho_g)\sigma}. \quad (9)$$

Because the present data correspond to saturated inlet conditions, the criterion for negating the influence of gravity perpendicular to the heated wall is a function of inlet quality, $x_{e,in}$. To develop a criterion that a designer can employ without solving the detailed two-phase flow field, a two-step approach is used. First, the criterion is examined by replacing (U_g-U_f) in Eqs. (7) and (9) by the known G/ρ_f Next, the criterion is modified to account for $x_{e,in}$.

Fig. 9(a) and (b) showed how CHF is greatly influenced by orientation for low values of G/ρ_f, especially for low inlet quality. By increasing inlet velocity and quality, the variation in CHF between orientations is shown to diminish. To develop a systematic criterion for negating the influence of orientation, CHF data such as those shown in Fig. 9(a) and (b) are filtered to determine, for each value of G/ρ_f and $x_{e,in}$, if the CHF variations with orientation falls within ±25% of the average CHF for all orientations. Evidenced by the trends in Fig. 9(a) and (b), low values of G/ρ_f do not satisfy this criterion. Fig. 12 shows, for all test conditions, the locus of minimum G/ρ_f values that satisfy the ±25% criterion decreases with increasing $x_{e,in}$. Also shown in the same figure are the data points that do satisfy the minimum CHF variation. Notice that $G/\rho_f=1.13$ and 0.995 m/s show minimum dependence on orientation for all inlet qualities. For $G/\rho_f=0.853$ m/s, the influence of orientation is negligible for $x_{e,in}\geqslant 0.03$ but begins to fall outside of the ±25% bounds at $x_{e,in}=0.01$. Proceeding to $G/\rho_f=0.712$ and 0.542 m/s, the quality required to negate the influence of orientation increases to $x_{e,in}=0.07$ and 0.13, respectively. For $G/\rho_f\leqslant 0.398$ m/s, fluid inertia is far too weak to overcome orientation effects even at high inlet qualities. The locus of minimum G/ρ_f values necessary to negate orientation effects is fitted by the relation

$$\left.\frac{G}{\rho_f}\right|_{\min}=0.584e^{(-15.75x_{e,in})}+0.496, \quad (10)$$

with a mean absolute error (MAE) of 2.17%. For $x_{e,in}=0$, Eq. (10) predicts a minimum G/ρ_f of 1.08 m/s.

Fig. 13(a) and (b) show the variations of Bo/We^2 with orientation and velocity, where (U_g-U_f) is substituted by G/ρ_f. For a fixed G/ρ_f, the magnitude of Bo/We^2 is highest for horizontal flows, $\theta=0°$ and 180°, where $|\cos\theta|=1$, and lowest for vertical flows, $\theta=90°$ and 270°, where $\cos\theta=0$. Notice in Fig. 13(a) how the influence of gravity is quite pronounced for $G/\rho_f=0.126$ and 0.224 m/s but decreases appreciably for $G/\rho_f\geqslant 0.398$ m/s. Fig. 13(b) shows variations of Bo/We^2 for $G/\rho_f\geqslant 0.398$ m/s, where low values of Bo/We^2 point to a very weak influence of orientation for high mass velocities.

Zhang et al. [29] developed a Bo/We^2 criterion for negating the influence of body force perpendicular to the heated wall for $x_{e,in}\leqslant 0$ based on $G/\rho_f=1.5$ m/s, for which their database showed minimum CHF dependence on orientation. Since the present database encompasses a broad range of $x_{e,in}$, a new Bo/We^2 criterion is developed using only data for which G/ρ_f exceeds the minimum criterion given by Eq. (10). Fig. 13(c) shows values of Bo/We^2 for conditions that negate orientation effects are represented for $|\cos\theta|=1$ (corresponding to strongest orientation influence) by the relation

$$\frac{Bo}{We^2}=\frac{(\rho_f-\rho_g)(\rho_f+\rho_g)^2\sigma g_e}{\rho_f^2\rho_g^2(G/\rho_f)^4}\leq 0.230e^{(-67.03x_{e,in})}+0.00249. \quad (11)$$

5.3. Criterion for negating influence of gravity component parallel to heated wall

Zhang et al. [29] developed a criterion for negating the influence of gravity parallel to the heated wall and opposite to the fluid flow using an expression for rise velocity for a large coalescent slug bubble relative to liquid [46],

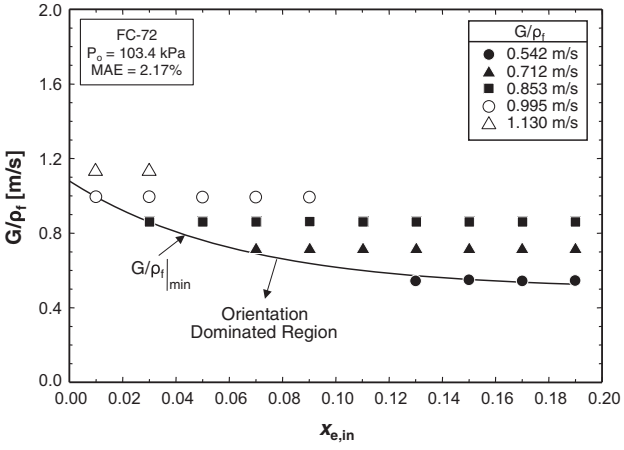

Fig. 12. Determination of minimum G/ρ_f necessary to negate effects of orientation on CHF for different inlet qualities.

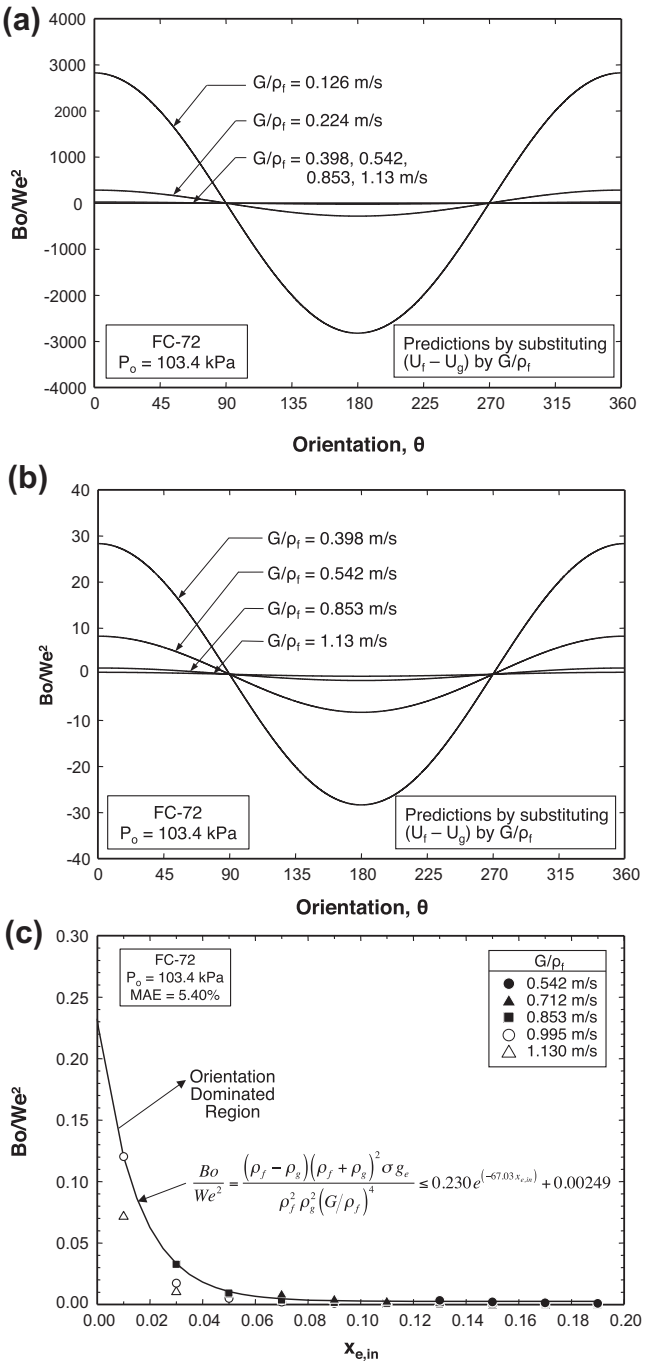

Fig. 13. Variation of Bo/We^2 with mass velocity and orientation for (a) all mass velocities and (b) $G/\rho_f \geq 0.398$ m/s. (c) Determination of Bo/We^2 criterion for negating influence of gravity perpendicular to heated wall.

$$U_\infty = 0.35\frac{[(\rho_f-\rho_g)g_e|\sin\theta|D_h]^{1/2}}{\rho_f^{1/2}}. \tag{12}$$

When U_∞ exceeds the liquid velocity, $U_{f,in}$, the vapor tends to flow backwards relative to the liquid, and vapor stagnation along the channel will occur when the two velocities are equal. The *Vapor Backflow* and *Vapor Stagnation Regimes* are associated with flooding as indicated for $G/\rho_f = 0.126$ m/s in Fig. 11. A sufficient criterion for negating flooding regimes $U_\infty < U_{f,in}$, which, for $\sin\theta = 1$ (corresponding to strongest orientation influence), can be presented in terms of the Froude number,

$$\left|\frac{1}{Fr}\right| = \left|\frac{(\rho_f-\rho_g)g_eD_h}{\rho_fU_{f,in}^2}\right| \leq 8.16. \tag{13}$$

As discussed earlier, because $x_{e,in} > 0$ in the present study, determining $U_{f,in}$ in Eq. (13) requires solving the detailed two-phase flow field. Therefore, the $1/Fr$ criterion is developed in a two-step approach. First, the criterion is examined by replacing $U_{f,in}$ by the known G/ρ_f. Next, the criterion is modified to account for $x_{e,in}$.

Fig. 14(a) and (b) show the variations of $1/Fr$ for different flow velocities and orientations in the range of $180° < \theta < 360°$ prone to flooding, where $U_{f,in}$ is replaced by G/ρ_f. The two figures show the influence of gravity on $1/Fr$ greatly decreases with increasing G/ρ_f. Like the Bo/We^2 criterion, this proves that high mass velocity is the most effective means to overcoming flooding effects. Fig. 14(c) shows values of $1/Fr$ for G/ρ_f values that negate orientation effects are represented, for $\sin\theta = 1$ (corresponding to strongest orientation influence), by the relation

$$\frac{1}{Fr} = \frac{(\rho_f-\rho_g)g_eD_h}{\rho_f(G/\rho_f)^2} \leq 0.0184e^{(-37.07x_{e,in})} + 0.0016. \tag{14}$$

5.4. Criterion for critical wavelength compared to heated length

Even when the criterion for negating the influence of gravity perpendicular to the heated wall is satisfied, it is crucial that the interfacial wavelength be smaller than the heated length, *i.e.*, $\lambda_c \leqslant L$, to enable liquid contact with the heated wall. Using the expression for λ_c from Eq. (6), this criterion can be expressed as a Weber number criterion,

$$We = \frac{\rho_f\rho_g(U_g-U_f)^2L}{(\rho_f+\rho_g)\sigma} \geq 2\pi. \tag{15}$$

As with the previous two criteria, the heated length criterion is modified by replacing $(U_g - U_f)$ in the definition of We by G/ρ_f. Next, the criterion is modified to account for $x_{e,in}$ by examining only G/ρ_f values that negate orientation effects as shown in Fig. 15(a),

$$We = \frac{\rho_f\rho_g(G/\rho_f)^2L}{(\rho_f+\rho_g)\sigma} \geq 1015e^{(8.682x_{e,in})} - 595.2. \tag{16}$$

5.5. Dominant mechanism for negating gravity effects

Notice that Eqs. (11), (14), and (16) point to increasing G/ρ_f as the most effective means to satisfying all three criteria for negating the influence of gravity on CHF. The same equations prove that a smaller G/ρ_f is required when increasing $x_{e,in}$. The three criteria are now combined to determine which criterion is dominant for different gravity fields, and the corresponding minimum G/ρ_f. This minimum value is of paramount importance to thermal management in both terrestrial and space applications since it corresponds to the minimum pumping power required to prevent CHF while avoiding the aforementioned flow anomalies.

Fig. 15(b) shows the minimum mass velocity required to satisfy each of the three criteria as a function of g/g_e, the prevailing gravity nondimensionalized by Earth's gravity. For each of the three criteria, G/ρ_f is computed for a range of $x_{e,in}$ values.

For subcooled conditions ($x_{e,in} \leqslant 0$), the minimum G/ρ_f is dominated by the flooding criterion (gravity component parallel to heated wall) for $g/g_e > 1.2$, and instability criterion (gravity component perpendicular to heated wall) for $g/g_e < 1.2$. The heated length criterion is dominant only for very small values of g/g_e, including microgravity, and the transition between this criterion and the instability criterion is a function of the heated length, with shorter length requiring a greater G/ρ_f. Notice that the minimum G/ρ_f in

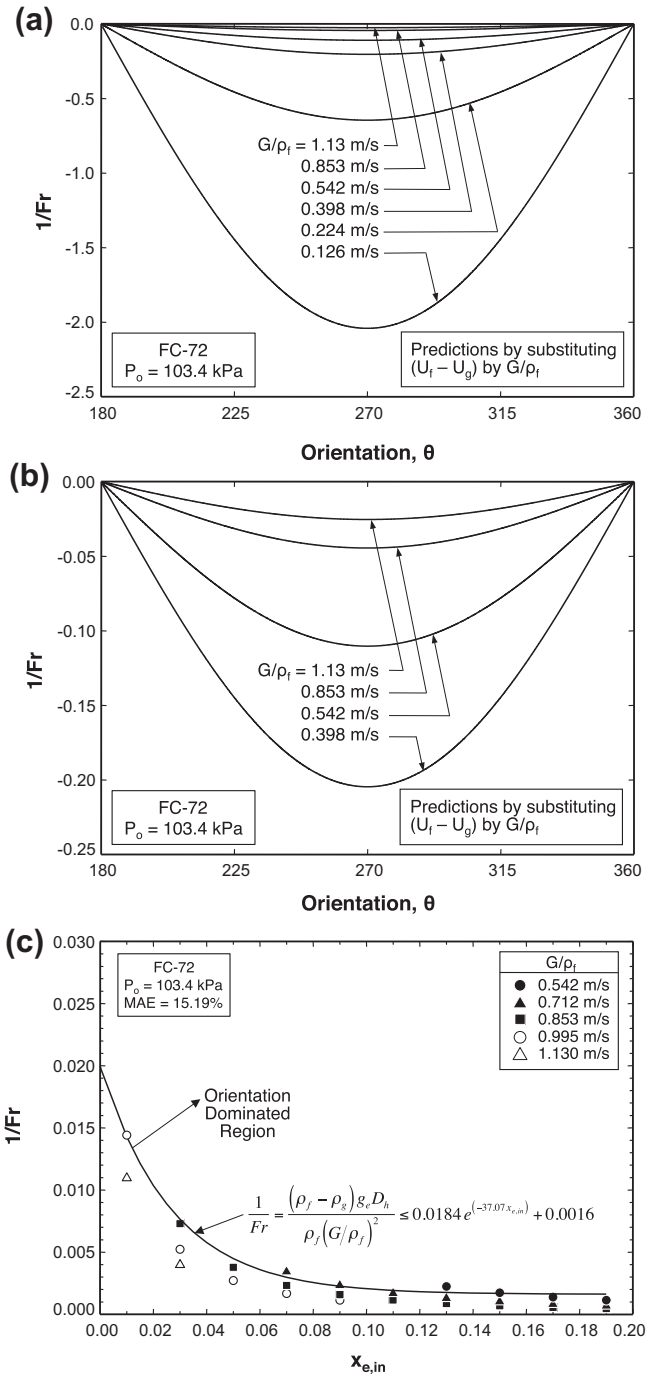

Fig. 14. Variation of *1/Fr* with mass velocity and orientation in the range of 180–360° for (a) all mass velocities and (b) $G/\rho_f \geq 0.398$ m/s. (c) Determination of *1/Fr* criterion for negating influence of gravity parallel to heated wall.

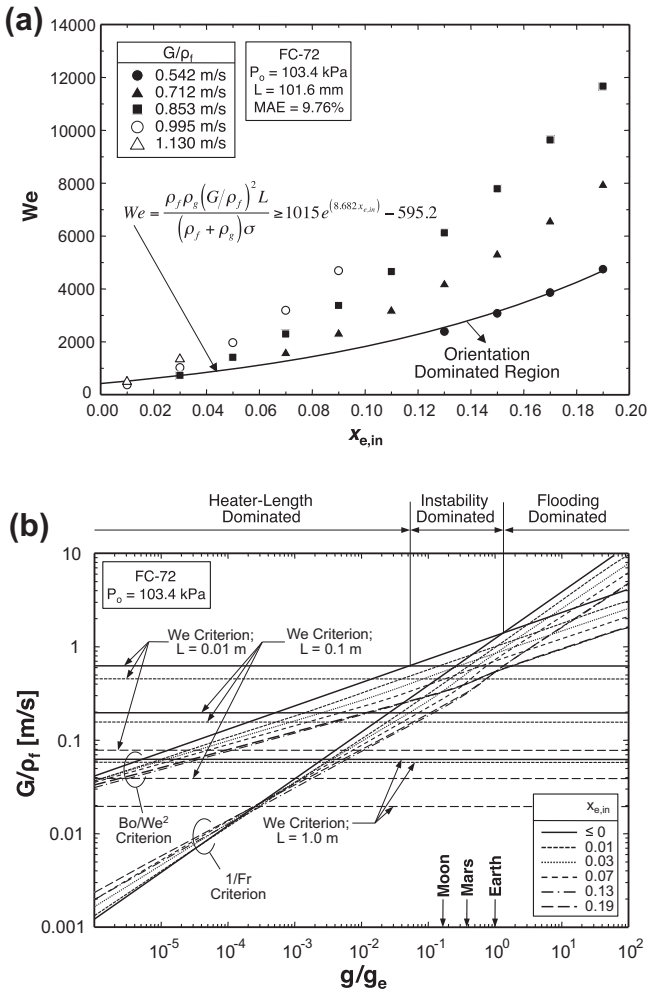

Fig. 15. Determination of (a) *We* criterion related to heated length versus critical wavelength, and (b) minimum G/ρ_f required to overcome all gravity effects on CHF.

Lunar, Martian and Earth environments is dominated by the instability criterion. Fig. 15(b) shows that the minimum G/ρ_f decreases monotonically with increasing $x_{e,in}$ for all three criteria.

6. Conclusions

This study explored the influence of orientation on flow boiling CHF with two-phase inlet conditions. Using FC-72 as working fluid, different CHF regimes were identified for different orientations, mass velocities and inlet qualities. These results were used to develop dimensionless criteria for negating the influence of gravity on CHF. Key findings from the study are as follows:

1. Orientation has an appreciable influence on CHF for low mass velocities ($G/\rho_f \leqslant 0.224$ m/s), resulting in a number of CHF regimes, including *Pool Boiling, Stratification* and *Wavy Vapor Layer*. On the other hand, only the *Wavy Vapor Layer Regime* is prevalent at high mass velocities. Overall, the influence of orientation on CHF is insignificant in the limit of very high mass velocity, especially with high inlet quality.
2. Negating the influence of orientation on CHF is achieved by simultaneously satisfying three separate criteria: overcoming the influence of gravity perpendicular to the heated wall, overcoming the influence of gravity parallel to the heated wall, and ensuring that the wavelength of the liquid–vapor interface is smaller than the heated wall to facilitate liquid contact with wall.
3. The three criteria for negating the influence of orientation on CHF can be combined to determine the minimum mass velocity required to negate gravity effects in any gravitational environment. This minimum is crucial to the design of thermal management systems in both terrestrial and space applications since it corresponds to the minimum pumping power required to operate safely below CHF.

Acknowledgment

The authors are grateful for the support of the National Aeronautics and Space Administration (NASA) under Grant no. NNX13AC83G.

References

[1] F.P. Chiaramonte, J.A. Joshi, Workshop on critical issues in microgravity fluids, transport, and reaction processes in advanced human support technology – final report, NASA TM-2004-212940, 2004.

[2] The National Academies, Recapturing a future for space exploration: life and physical sciences research for a new era, National Academies Press, Washington, DC, 2011.

[3] Zuber, M., Tribus, J.W. Westwater, The hydrodynamic crisis in pool boiling of saturated and subcooled liquids, in: Int. Dev. Heat Transfer: Proc. 1961–62 Int. Heat Transfer Conf., Boulder, CO, 1961, pp. 230–236.

[4] T.M. Anderson, I. Mudawar, Microelectronic cooling by enhanced pool boiling of a dielectric fluorocarbon liquid, J. Heat Transfer Trans. ASME 111 (1989) 752–759.

[5] R.A. DeBortoli, S.J. Green, B.W. LeTourneau, M. Troy, A. Weiss, Forced-Convection Heat Transfer Burn-Out Studies for Water in Rectangular and Round Tubes at Pressures Above 500 Psia, WAPD-188, Westinghouse Electric Corp., Pittsburgh, PA, 1958.

[6] A.P. Ornatskii, L.S. Vinyarskii, Heat transfer crisis in a forced flow of underheated water in small-bore tubes, High Temp. 3 (1965) 400–406.

[7] T.C. Willingham, I. Mudawar, Forced-convection boiling and critical heat flux from a linear array of discrete heat sources, Int. J. Heat Mass Transfer 35 (1992) 2879–2890.

[8] D.D. Hall, I. Mudawar, Ultra-high critical heat flux (CHF) for subcooled water flow boiling – II. High-CHF database and design parameters, Int. J. Heat Mass Transfer 42 (1999) 1429–1456.

[9] D.D. Hall, I. Mudawar, Critical heat flux (CHF) for water flow in tubes – I. Compilation and assessment of world CHF data, Int. J. Heat Mass Transfer 43 (2000) 2573–2604.

[10] D.D. Hall, I. Mudawar, Critical heat flux (CHF) for water flow in tubes – II. Subcooled CHF correlations, Int. J. Heat Mass Transfer 43 (2000) 2605–2640.

[11] Y. Katto, M. Kunihiro, Study of the mechanism of burn-out in boiling system of high burn-out heat flux, Bull. JSME 16 (1973) 1357–1366.

[12] M. Monde, T. Inoue, Critical heat flux in saturated forced convective boiling on a heated disk with multiple impinging jets, J. Heat Transfer Trans. ASME 113 (1991) 722–727.

[13] D.C. Wadsworth, I. Mudawar, Enhancement of single-phase heat transfer and critical heat flux from an ultra-high-flux-source to a rectangular impinging jet of dielectric liquid, J. Heat Transfer Trans. ASME 114 (1992) 764–768.

[14] M.E. Johns, I. Mudawar, An ultra-high power two-phase jet-impingement avionic clamshell module, J. Electron. Packag. Trans. ASME 118 (1996) 264–270.

[15] S. Toda, A study in mist cooling (lst report: investigation of mist cooling), Trans. JSME 38 (1972) (1972) 581–588.

[16] L. Lin, R. Ponnappan, Heat transfer characteristics of spray cooling in a closed loop, Int. J. Heat Mass Transfer 46 (2003) 3737–3746.

[17] J.R. Rybicki, I. Mudawar, Single-phase and two-phase cooling characteristics of upward-facing and downward-facing sprays, Int. J. Heat Mass Transfer 49 (2006) 5–16.

[18] W. Nakayama, T. Nakajima, S. Hirasawa, Heat sink studs having enhanced boiling surfaces for cooling of microelectronic components, ASME Paper 84-WA/HT-89, 1984.

[19] R.L. Webb, The evolution of enhanced surface geometries for nucleate boiling, Heat Transfer Eng. 2 (1981) 46–69.

[20] V. Khanikar, I. Mudawar, T. Fisher, Effects of carbon nanotube coating on flow boiling in a micro-channel, Int. J. Heat Mass Transfer 52 (2009) 3805–3817.

[21] S.S. Kutateladze, A.I. Leont'ev, Some applications of the asymptotic theory of the turbulent boundary layer, in: Proc. Third Int. Heat Transfer Conf., Chicago, Illinois, vol. 3, 1966, pp. 1–6.

[22] L.S. Tong, Boundary-layer analysis of the flow boiling crisis, Int. J. Heat Mass Transfer 11 (1968) 1208–1211.

[23] W. Hebel, W. Detavernier, M. Decreton, A contribution to the hydrodynamics of boiling crisis in a forced flow of water, Nucl. Eng. Des. 64 (1981) 443–445.

[24] J. Weisman, B.S. Pei, Prediction of critical heat flux in flow boiling at low qualities, Int. J. Heat Mass Transfer 26 (1983) 1463–1477.

[25] C.H. Lee, I. Mudawar, A mechanistic critical heat flux model for subcooled flow boiling based on local bulk flow conditions, Int. J. Multiphase Flow 14 (1988) 711–728.

[26] J.E. Galloway, I. Mudawar, CHF mechanism in flow boiling from a short heated wall-part 1. Examination of near-wall conditions with the aid of photomicrography and high-speed video imaging, Int. J. Heat Mass Transfer 36 (1993) 2511–2526.

[27] J.E. Galloway, I. Mudawar, CHF mechanism in flow boiling from a short heated wall-part 2. Theoretical CHF model, Int. J. Heat Mass Transfer 36 (1993) 2527–2540.

[28] H. Zhang, I. Mudawar, M.M. Hasan, Experimental assessment of the effects of body force, surface tension force, and inertia on flow boiling CHF, Int. J. Heat Mass Transfer 45 (2002) 4079–4095.

[29] H. Zhang, I. Mudawar, M.M. Hasan, A method for assessing the importance of body force on flow boiling CHF, J. Heat Transfer Trans. ASME 126 (2004) 161–168.

[30] J.C. Sturgis, I. Mudawar, Critical heat flux in a long, rectangular channel subjected to onesided heating – I. Flow visualization, Int. J. Heat Mass Transfer 42 (1999) 1835–1847.

[31] J.C. Sturgis, I. Mudawar, Critical heat flux in a long, rectangular channel subjected to onesided heating – II. Analysis of critical heat flux data, Int. J. Heat Mass Transfer 42 (1999) 1849–1862.

[32] R.J. Simoneau, F.F. Simon, A visual study of velocity and buoyancy effects on boiling Nitrogen, NASA Tech Note TN D-3354, 1966.

[33] K. Mishima, H. Nishihara, The effect of flow direction and magnitude on CHF for low pressure water in thin rectangular channels, Nucl. Eng. Des. 86 (1985) 165–181.

[34] C.O. Gersey, I. Mudawar, Effects of heater length and orientation on the trigger mechanism for near-saturated flow boiling critical heat flux – I. Photographic study and statistical characterization of the near-wall interfacial features, Int. J. Heat Mass Transfer 38 (1995) 629–641.

[35] C.O. Gersey, I. Mudawar, Effects of heater length and orientation on the trigger mechanism for near-saturated flow boiling critical heat flux – II. Critical heat flux model, Int. J. Heat Mass Transfer 38 (1995) 643–654.

[36] H. Zhang, I. Mudawar, M.M. Hasan, Flow boiling CHF in microgravity, Int. J. Heat Mass Transfer 48 (2005) 3107–3118.

[37] I. Mudawar, A.H. Howard, C.O. Gersey, An analytical model for near-saturated pool boiling CHF on vertical surfaces, Int. J. Heat Mass Transfer 40 (1997) 2327–2339.

[38] A.H. Howard, I. Mudawar, Orientation effects on pool boiling CHF and modeling of CHF for near-vertical surfaces, Int. J. Heat Mass Transfer 42 (1999) 1665–1688.

[39] A.H. Howard, I. Mudawar, Photographic study of pool boiling CHF from a downward-facing convex surface, Int. Commun. Heat Mass Transfer 35 (2008) 793–799.

[40] C.R. Kharangate, I. Mudawar, M.H. Hasan, Experimental and theoretical study of critical heat flux in vertical upflow with inlet vapor void, Int. J. Heat Mass Transfer 55 (2012) 360–374.

[41] C.R. Kharangate, I. Mudawar, M.H. Hasan, Photographic study and modeling of critical heat flux in horizontal flow boiling with inlet vapor void, Int. J. Heat Mass Transfer 55 (2012) 4154–4168.

[42] C. Konishi, I. Mudawar, Investigation of the influence of orientation on critical heat flux for flow boiling with two-phase inlet, Int. J. Heat Mass Transfer 61 (2013) 176–190.

[43] Z. Nejat, Effect of density ratio on critical heat flux in closed end vertical tubes, Int. J. Multiphase Flow 7 (1981) 321–327.

[44] H. Lamb, Hydrodynamics, sixth ed., Dover Publications, NY, 1945.

[45] L.M. Milne-Thompson, Theoretical Hydrodynamics, fourth ed., Macmillan, NY, 1960.

[46] G.B. Wallis, One-Dimensional Two-Phase Flow, McGraw Hill Book Company, New York, 1969.